J|A|C|S
ARTICLES
Published on Web 03/12/2002

Intra- and Intermolecular Topological Properties of Amino Acids: A Comparative Study of Experimental and Theoretical Results

R. Flaig,[†] T. Koritsanszky,[‡] B. Dittrich,[†] A. Wagner,[†] and P. Luger*,[†]

Contribution from the Institute for Chemistry/Crystallography, Free University of Berlin, Takustrasse 6, 14195 Berlin, Germany, and Department of Chemistry, State University of New York at Buffalo, Buffalo New York 14260

Received June 18, 2001

Abstract: The charge densities $\rho(\mathbf{r})$ of the six amino acids L-Asn·H_2O, DL-Glu·H_2O, DL-Lys·HCl, DL-Pro·H_2O, DL-Ser, and DL-Val were determined from high-resolution X-ray diffraction experiments at 100 K using synchrotron radiation and area detection (CCD) techniques. Bond topological parameters derived from these densities and from those of six additional amino acids published earlier are compared to each other and to the results of ab initio calculations. Experimental and theoretical properties for each chemically equivalent bond are in a fair agreement, and their variances are of similar magnitude. A noticeable outlier is the positive curvature of the density at the bond critical point, for which no correlation between the experimental and theoretical values can be established. The location of nonbonded valence shell charge concentrations derived from the crystalline densities scatter in a wider range than those obtained for the isolated molecules.

1. Introduction

The solid-state electron density $\rho(\mathbf{r})$ can be obtained experimentally by high-resolution X-ray diffraction.[1] Although the method of charge density determination has been known since the 1960s, the time-consuming nature of data collection has limited earlier applications to smaller molecules. Due to the application of area detectors, intense synchrotron radiation at a short wavelength ($\lambda \approx 0.5$ Å), and stable cooling devices, it is now possible to collect X-ray data of high resolution and precision within a reasonable time, allowing even comparative studies on an entire class of chemically related compounds.[2]

In Bader's theory of "Atoms in Molecules" (AIM)[3] the charge density plays a central role. On the basis of the topology of this scalar field the concept of atoms, functional groups, and chemical bonds can unambiguously be defined, and atomic interactions be characterized in terms of a limited number of topological descriptors. In this context it is an important question whether atomic properties can be used to construct molecular ones, that is, to what extent submolecular topological properties are transferable to larger systems. Bader et al. have studied the possibility of theoretical construction of polypeptides. They have shown that the properties of some di- and tripeptides can be successfully predicted from those corresponding to the constituent peptide groups.[4,5] A complementary approach to the construction of biopolymers from monomers makes use of the apparent transferability of multipole populations.[6−9]

The experimenal verification of the topological approach is the objective of numerous studies comparing bond topological properties (BTP) based on X-ray charge density with those derived from a wave function.[10] Among the properties examined in detail the density at the bond critical point ($\mathbf{r_{BCP}}$, where $\nabla\rho(\mathbf{r_{BCP}}) = 0$) is the most reproducible. While the agreement between theory and experiment in terms of curvatures perpendicular to covalent bonds was found to be satisfactory in most of the cases, considerable differences have been obtained in terms of parallel curvatures and consequently, in terms of the Laplacian ($\nabla^2\rho(\mathbf{r_{BCP}})$), especially for polar bonds. Recent results suggest that the main source of this disagreement is the limited flexibility of the density radial functions applied to interpret the diffraction data.[11] In this report we summarize the results of topological analyses of theoretical and experimental densities of six amino acids (L-Asn·H_2O, DL-Glu·H_2O, DL-Lys·HCl, DL-Pro·H_2O, DL-Ser, and DL-Val) and compare them with those of

* Author for correspondence. E-mail: luger@chemie.fu-berlin.de.
[†] Free University of Berlin.
[‡] State University of New York at Buffalo.

(1) Coppens P. *X-ray Charge Densities and Chemical Bonding*; Oxford University Press: New York, 1997.
(2) Koritsanszky, T.; Flaig, R.; Zobel, D.; Krane, H.-G.; Morgenroth, W.; Luger, P. *Science* **1998**, *279*, 356−358.
(3) Bader, R. F. W. *Atoms in Molecules: A Quantum Theory*, 1st ed.; No. 22 in The International Series of Monographs on Chemistry; Clarendon Press: Oxford: London, 1990.
(4) Popelier, P. L. A.; Bader, R. F. W. *J. Phys. Chem.* **1994**, *98*, 4473−4481.
(5) Chang, C.; Bader, R. F. W. *J. Phys. Chem.* **1992**, *96*, 1654−1662.
(6) Pichon-Pesme, V.; Lecomte, C.; Wiest, R.; Bénard, M. *J. Am. Chem. Soc.* **1992**, *114*, 2713−2715.
(7) Pichon-Pesme, V.; Lecomte, C.; Lachekar, H. *J. Phys. Chem.* **1995**, *99*, 6242−6250.
(8) Jelsch, C.; Pichon-Pesme, V.; Lecomte, C.; Aubry, A. *Acta Crystallogr., Sect. D* **1998**, *54*, 1306−1318.
(9) Jelsch, C.; Teeter, M. M.; Lamzin, V.; Pichon-Pesme, V.; Blessing, R. H.; Lecomte, C. *Proc. Natl. Acad. Sci. U.S.A.* **2000**, *97*, 3171−3176.
(10) Koritsanszky, T.; Coppens, P. *Chem. Rev.* **2001**, *101*, 1583−1627.
(11) Volkov, A.; Abramov, Y.; Coppens, P.; Gatti, C. *Acta Crystallogr., Sect. A* **2000**, *A56*, 332−339.

Table 1. Crystallographic Data and Figures of Merit

	Asn	Glu	Lys	Pro	Ser	Val
formula	$C_4O_3N_2H_8 \cdot H_2O$	$C_5O_4NH_9 \cdot H_2O$	$C_6O_2N_2H_{15}^+Cl^-$	$C_5O_2NH_9 \cdot H_2O$	$C_3O_3NH_7$	$C_5O_2NH_{11}$
crystal system	orthorhombic	orthorhombic	monoclinic	orthorhombic	monoclinic	triclinic
space group	$P2_12_12_1$ (No. 19)	*Pbca* (No. 61)	$P2_1/c$ (No. 14)	*Pbca* (No. 61)	$P2_1/a$ (No. 14)	$P\bar{1}$ (No. 2)
Z	4	8	4	8	4	2
a [Å]	5.580(3)	9.080(3)	9.157(1)	5.253(3)	10.756(5)	5.2330(2)
b [Å]	9.743(2)	15.401(2)	11.166(2)	11.987(5)	9.172(4)	5.4145(2)
c [Å]	11.706(2)	10.612(2)	8.547(1)	19.864(1)	4.788(4)	10.8302(4)
α [deg]	90.0	90.0	90.0	90.0	90.0	90.834(3)
β [deg]	90.0	90.0	105.83(3)	90.0	106.73(3)	92.291(3)
γ [deg]	90.0	90.0	90.0	90.0	90.0	110.098(3)
V [Å^3]	636.38	1484.01	840.66	1250.84	452.5	287.82
D_x [g·cm^{-3}]	1.567	1.478	1.443	1.414	1.543	1.352
λ[Å]	0.5296	0.5296	0.5000	0.4960	0.4500	0.4500
μ[mm^{-1}]	0.08	0.08	0.22	0.07	0.08	0.06
temperature [K]	100	100	100	100	100	100
$(\sin\theta/\lambda)_{max}$ [Å^{-1}]	1.46	1.30	1.38	1.12	1.54	1.54
reflections collected	58720	59716	70359	33742	49928	35468
unique reflections	11452	13940	15429	6758	11120	14403
R_{int}	0.0287	0.0440	0.0474	0.0430	0.0596	0.0492
reflections incl. in ref.	9972	9246	7970	5238	7127	9498
NVAR	331	337	310	310	295	253
R(*F*)	0.0333	0.0455	0.0333	0.0307	0.0362	0.0295
$R_w(F)$	0.0266	0.0347	0.0261	0.0208	0.0309	0.0302
GOF	1.89	1.89	1.69	1.34	1.40	1.18

our earlier investigations on DL-Asp,[12] L-Gln,[13] and L-Thr[14] and with those of investigations by other groups on Gly,[15] L-Ala,[16] L-Asn·H_2O,[17] and DL-His.[18] The topological data presented here cover 12 of the 20 naturally occurring amino acids and thus allow for a detailed comparison. Charge density studies including topological analyses on amino acid derivatives and small peptides have been published lately.[19−23]

2. Experimental Conditions

Crystals of the commercially available amino acids L-Asn, DL-Glu, DL-Lys·HCl, DL-Pro, DL-Ser and DL-Val were grown from aqueous solutions by vapor diffusion. X-ray data were collected at the beamlines F1 and D3 of the storage ring DORIS III at the HASYLAB/DESY, Hamburg, Germany, on a *κ*-axis (F1) and on a Huber four-circle diffractometer (at D3). For all measurements the temperature was maintained at 100 K with an Oxford Cryosystem N_2 gas stream cooling device. The CCD area detection (SMART 1000) allowed the measurement of several ten thousand reflections in beam-time periods of one or two days per sample. The frames were collected with a scan width of 0.05, 0.1, and 0.2° in *ω* and *φ*, respectively, and with exposure times in the range of 1−6 s. The detector-to-crystal distance was set to values between 3.5 and 4 cm. The measurement strategy was planned with ASTRO, the data collection was monitored with SMART, and the frames were integrated and corrected with the SAINT and SADABS programs.[24] Further details on the crystal data and the experimental conditions are given in Table 1.

3. Density Models and Refinement Strategy

The data were interpreted in terms of the generalized scattering factor model based on the Hansen−Coppens formalism.[25] The starting atomic parameters were taken from the spherical atom refinement (SHELXL).[26] Hydrogen-atom positions were kept fixed at idealized distances[27] since neutron data at the same temperature were not available. The multipole refinements were carried out with the full-matrix least-squares refinement program (XDLSM) of the XD program package.[28] In all cases the quantity $\sum_H w_H (F_{obs}(H) - k|F_{cal}(H)|)^2$ was minimized using the statistical weight $w_H = \sigma^{-2}(F_{obs}(H))$. The core and the spherical valence densities of the heavy atoms were composed of Hartree−Fock wave functions expanded over Slater-type basis functions, while the scattering factors of the hydrogen atoms were calculated from the exact radial density functions using *κ* values between 1.2 and 1.38. For the deformation terms single-*ζ* orbitals with energy-optimized Slater exponents were taken and kept fixed. The multipole expansion was truncated at the hexadecapolar level for carbon, nitrogen, and oxygen atoms, while the hydrogen atoms were represented by bond directed dipoles. A quadrupolar term was also included for hydrogen atoms involved in strong intermolecular interactions (DL-Glu·H_2O). The density of chemically equivalent atoms were kept to be the same. A local mirror symmetry was applied to the carbon atoms in the carboxylate and methylene groups, while C_{3v} symmetry was imposed for the methyl groups. No symmetry restriction was imposed on the nitrogen atom of the NH_3^+ group as it is involved in hydrogen bonding,

(12) Flaig, R.; Koritsanszky, T.; Zobel, D.; Luger, P. *J. Am. Chem. Soc.* **1998**, *120*, 2227−2238.
(13) Wagner, A.; Luger, P. *J. Mol. Struct. (THEOCHEM)* **2001**, *595*, 39−46.
(14) Flaig, R.; Koritsanszky, T.; Janczak, J.; Krane, H.-G.; Morgenroth, W.; Luger, P. *Angew. Chem., Int. Ed.* **1999**, *38*, 1397−1400.
(15) Destro, R.; Roversi, P.; Barzaghi, M.; Marsh, R. E. *J. Phys. Chem.* **2000**, *A104*, 1047−1054.
(16) Gatti, C.; Bianchi, R.; Destro, R.; Merati, F. *J. Mol. Struct. (THEOCHEM)* **1992**, *255*, 409−433.
(17) Arnold, W. D.; Sanders, L. K.; McMahon, M. T.; Volkov, A. V.; Wu, G.; Coppens, P.; Wilson, S. R.; Godbout, N.; Oldfield, E. *J. Am. Chem. Soc.* **2000**, *122*, 4708−4717.
(18) Coppens, P.; Abramov, Y.; Carducci, M.; Korjov, B.; Novozhilova, I.; Alhambra, C.; Pressprich, M. R. *J. Am. Chem. Soc.* **1999**, *121*, 2585−2593.
(19) Howard, S. T.; Hursthouse, B.; Lehmann, C. W.; Poyner, E. A. *Acta Crystallogr., Sect. B* **1995**, *51*, 328−337.
(20) Espinosa, E.; Lecomte, C.; Molins, E.; Veintemillas, S.; Cousson, A.; Paulus, W. *Acta Crystallogr., Sect. B* **1996**, *52*, 519−534.
(21) Dahaoui, S.; Pichon-Pesme, V.; Howard, J. A. K.; Lecomte, C. *J. Phys. Chem. A* **1999**, *103*, 6240−6250.
(22) Dittrich, B.; Flaig, R.; Koritsanszky, T.; Krane, H.-G.; Morgenroth, W.; Luger, P. *Chem. Eur. J.* **2000**, *6*, 2582−2589.
(23) Pichon-Pesme, V.; Lachekar, H.; Souhassou, M.; Lecomte, C. *Acta Crystallogr., Sect. B* **2000**, *56*, 728−737.
(24) Programs ASTRO 1995−1996, SMART 1996, SAINT 1994−1996, Bruker-AXS Inc.: Madison, WI.
(25) Hansen, N. K.; Coppens, P. *Acta Crystallogr., Sect. A* **1978**, *A34*, 909−921.
(26) Sheldrick, G. M. SHELXL, Crystal Structure Refinement; Universität Göttingen: Göttingen, 1997.
(27) Allen, F. H. *Acta Crystallogr., Sect. B* **1986**, *42*, 515−522.
(28) Koritsanszky, T.; Howard, S.; Richter, T.; Su, Z. W.; Mallinson, P. R.; Hansen, N. K. *XD: A Computer Program Package for Multipole Refinement and Analysis of Electron Densities from Diffraction Data. User manual*; Freie Universität Berlin: Berlin, 1995.

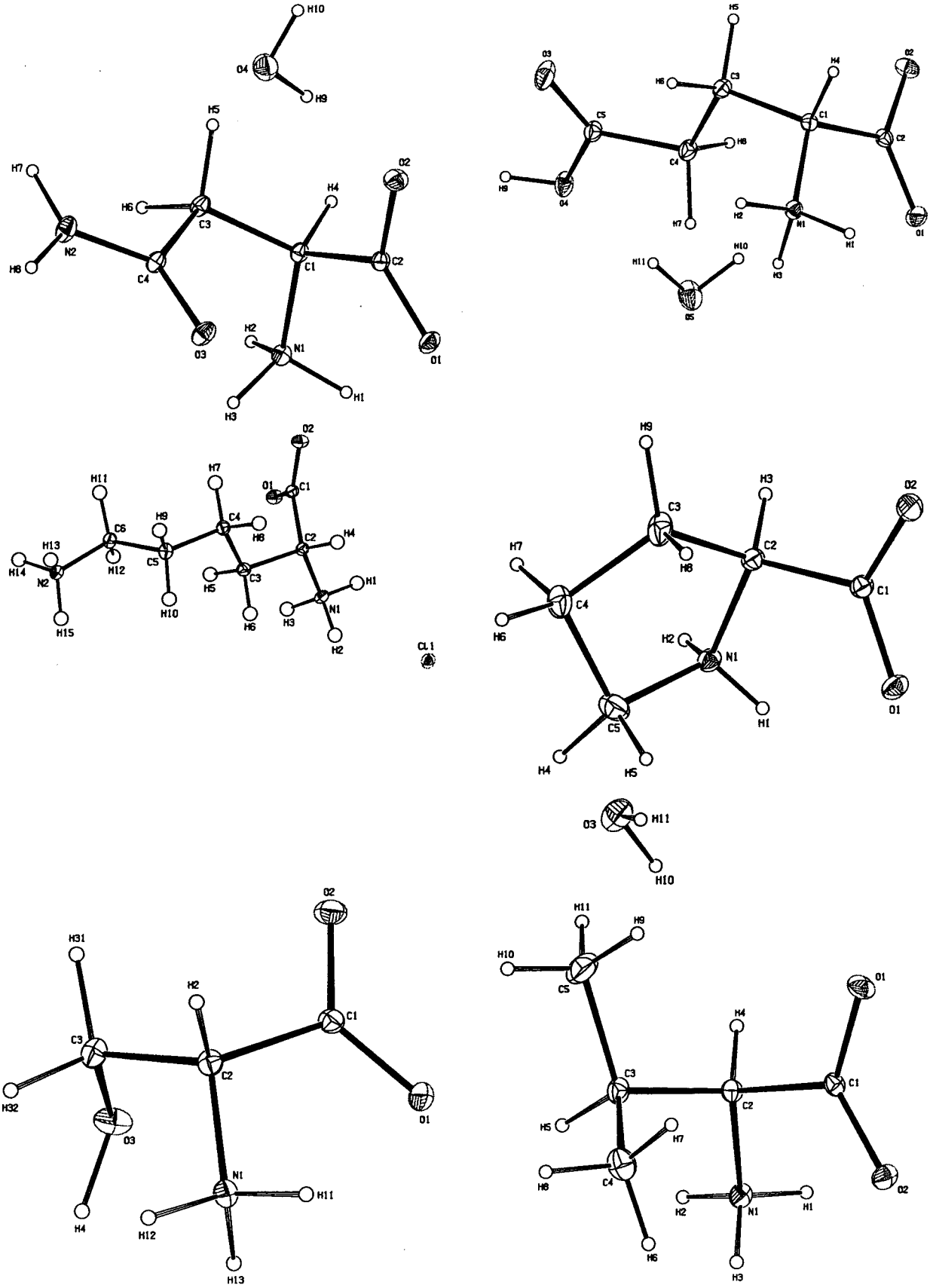

Figure 1. ORTEP representation of the six amino acids (50% probability) as derived from X-ray experiments.

but the densities of the hydrogen atoms attached to it were constrained to be the same. Only symmetry-independent reflections, which met the criterion $F_{obs}(H) > 3\sigma(F_{obs}(H))$, were included in the refinements. Agreement indices for the six data sets are listed in Table 1.

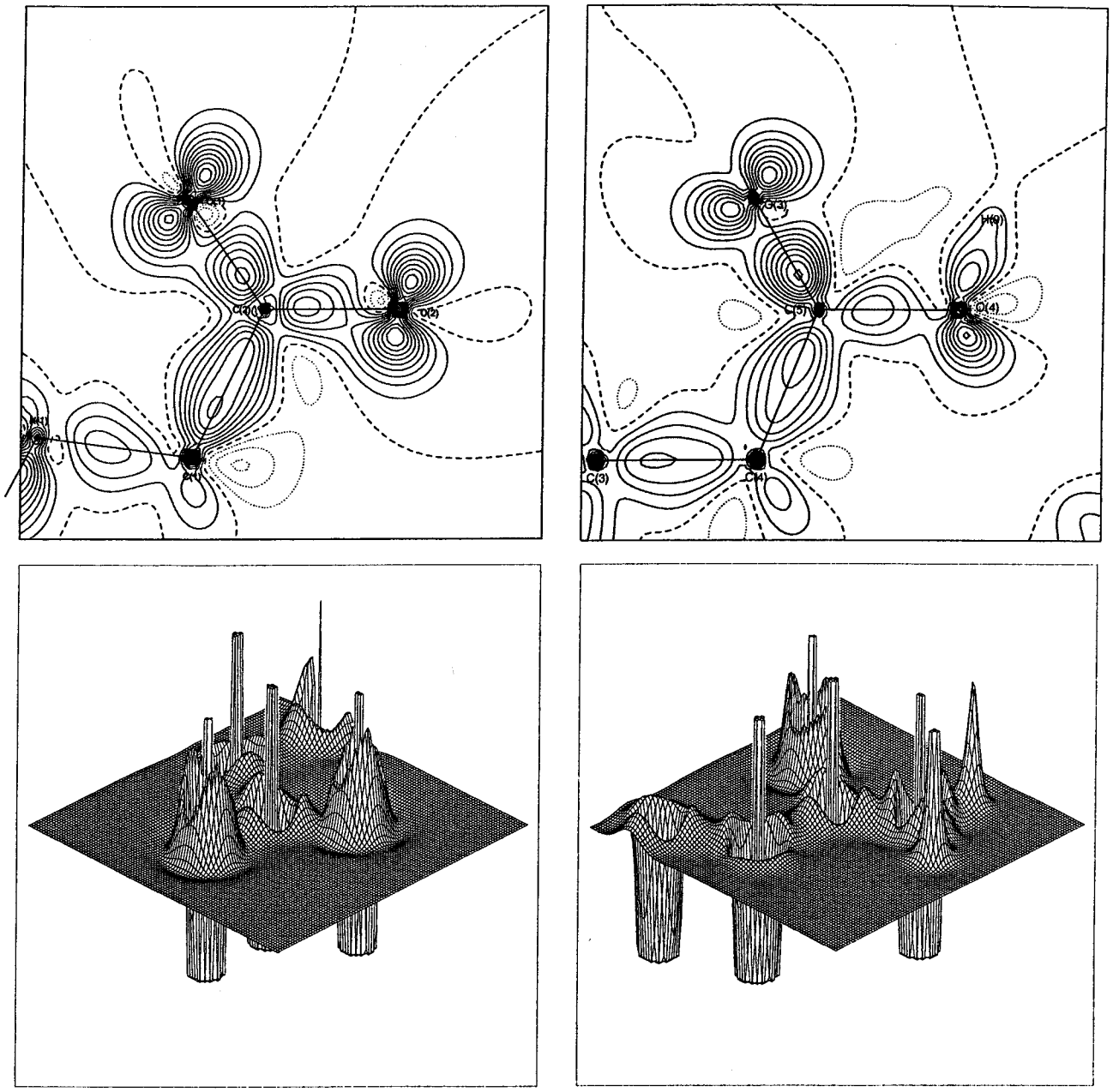

Figure 2. Static deformation densities for the COO^- and COOH groups (top) and relief representations of the negative Laplacian function for the COO^- and COOH groups (bottom) of glutamic acid.

4. Results and Discussion

The molecular structures of the six amino acids as derived from X-ray experiments are displayed as ORTEP[29] representations in Figure 1. To illustrate a few qualitative features the carboxyl and carboxylate groups of glutamic acid are displayed exemplarily by their static deformation density and Laplacian maps in Figure 2. The symmetric in-plane lone pair regions of the carboxyl oxygen atoms are clearly visible in both static maps. The out-of-plane lone pair of the hydroxyl oxygen is indicated by the maximum next to O(4). The three C−O bonds are noticably different. While the C−O(H) and the formal C═O bond in the COOH group show, respectively, the weakest and the strongest peak, the maxima on both C−O bonds of the COO^- group are in between. The Laplacian distributions in Figure 2 supports the qualitative findings revealed by the static deformation density maps. Both types of valence shell charge concentrations (VSCC) are clearly recognizable.

The zero Laplacian surfaces, designated as the reactive surfaces, of the six amino acids are displayed in Figure 3. Open spaces in these surfaces indicate local valence shell charge depletions, hence give detailed information on the reaction geometry and the preferred sites of nucleophilic attack. Common to all six amino acids are highly depleted regions at the carboxylate carbons and the carboxyl carbon (in glutamic acid). Further sites of preferred nucleophilic attack are at the carbon atoms of the amide group in Asn and in the C−OH group of Ser.

4.1. Topological Analysis. To explore theory versus experimental correlation ab initio calculations were performed with

(29) Burnett, M. N.; Johnson, C. K. *ORTEP-III, Oak Ridge Thermal Ellipsoid Plot Program for Crystal Structure Illustrations*; Oak Ridge National Laboratory Report ORNL-6895; Oak Ridge: Tennessee, 1996.

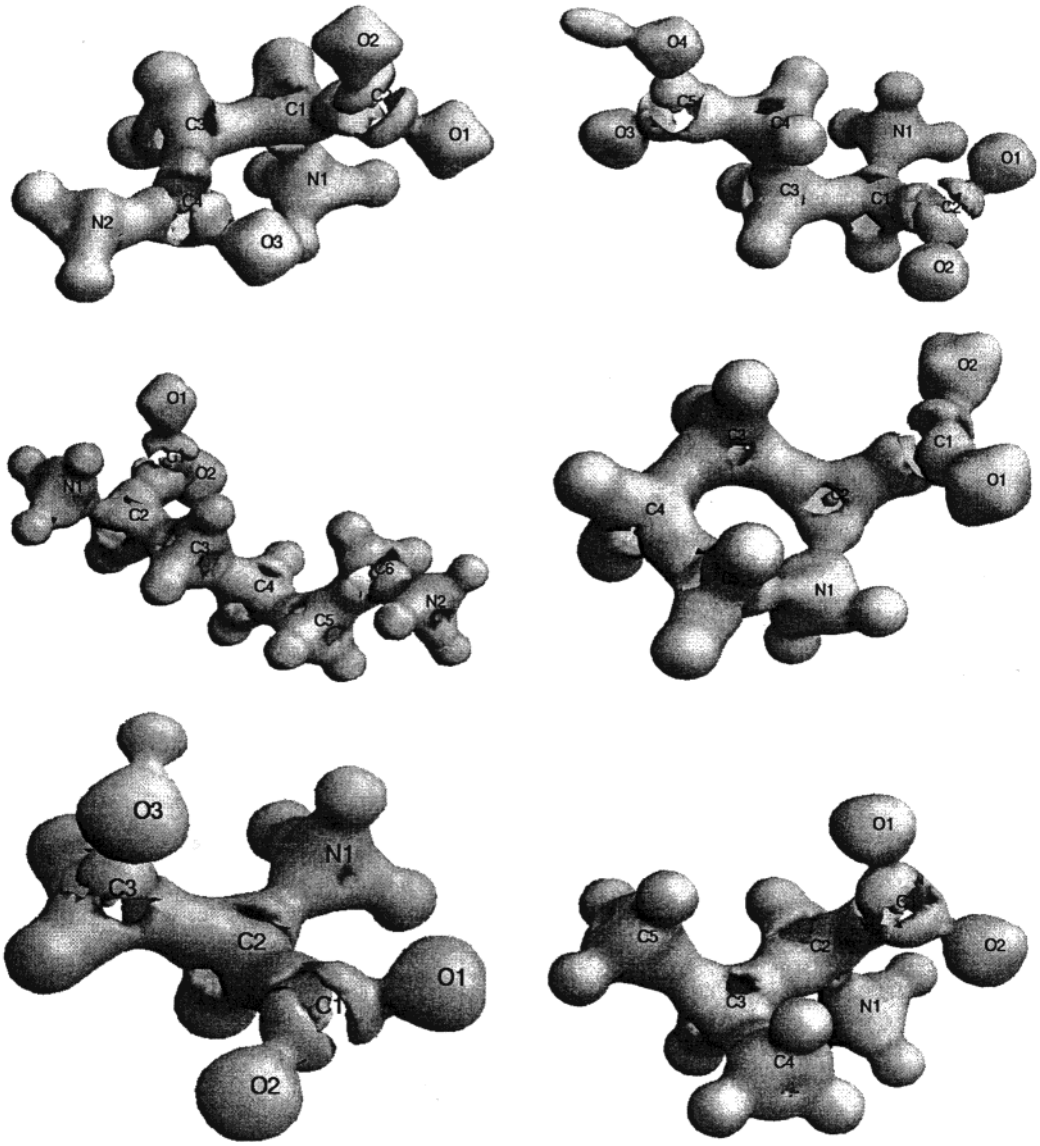

Figure 3. Zero Laplacian isosurfaces ($\nabla^2\rho(\mathbf{r}) = 0$) for L-Asn·$H_2O$ (top left), DL-Glu·H_2O (top right), DL-Lys·HCl (middle left), DL-Pro·H_2O (middle right), DL-Ser (bottom left) and DL-Val (bottom right).

Table 2. Average Experimental Bond Topological Properties with Standard Deviations in Brackets[a]

bond	average	N_{data}	ESD/average	bond	average	N_{data}	ESD/average
O(1)−C	2.71(9)	13	0.033	C−C_α	1.75(6)	13	0.034
	−33.6(45)	13	0.134		−13.0(22)	13	0.169
	0.791(17)	8	0.021		0.759(19)	8	0.025
	−26.4	13			−13.4	13	
	−23.4	13			−11.6	13	
	14.6	13			11.9	13	
O(2)−C	2.83(11)	13	0.039	C_α−C_β	1.68(8)	12	0.048
	−35.6(36)	13	0.101		−11.7(21)	12	0.179
	0.772(15)	8	0.019		0.778(16)	8	0.021
	−26.7	13			−12.1	12	
	−23.9	13			−11.2	12	
	15.7	13			11.6	12	
N−C_α	1.68(5)	13	0.030				
	−10.8(21)	13	0.194				
	0.853(17)	8	0.020				
	−13.2	13					
	−11.6	13					
	12.5	13					

[a] The first line denotes the value of $\rho(\mathbf{r}_c)$ [e/Å^3] at the BCP, the second line represents the value of $\nabla^2\rho(\mathbf{r}_c)$ [e/Å^5] at the BCP, the third line is the distance of the BCP from the first atom defining the bond [Å]. The fourth to the sixth line denote λ_1, λ_2, and λ_3 [e/Å^5], respectively.

O(1)–C(1)

$\overline{x} = 2.56(5), e/a = 0.020$

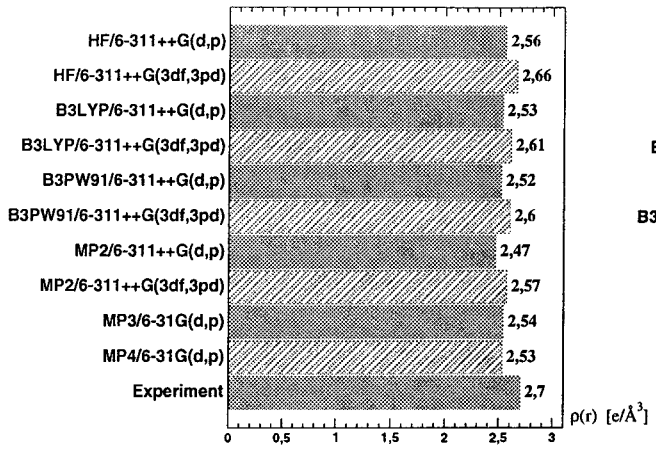

$\overline{x} = -13.5(42), e/a = 0.311$

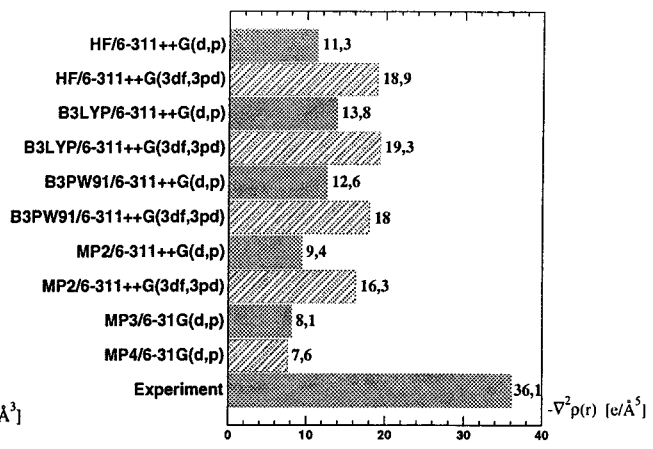

O(2)–C(1)

$\overline{x} = 2.59(5), e/a = 0.021$

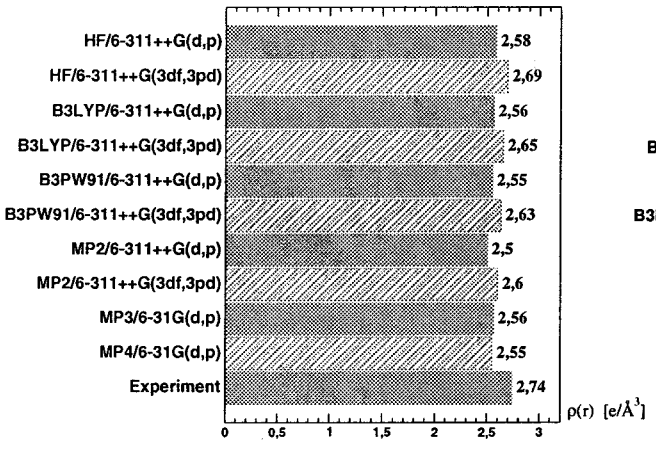

$\overline{x} = -10.5(48), e/a = 0.455$

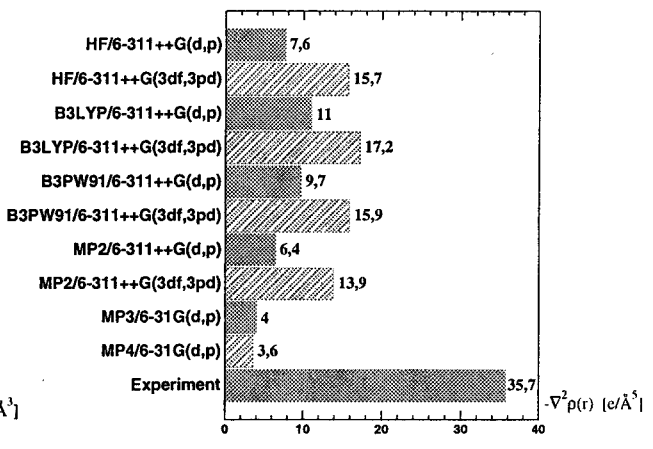

N–C_α

$\overline{x} = 1.55(2), e/a = 0.012$

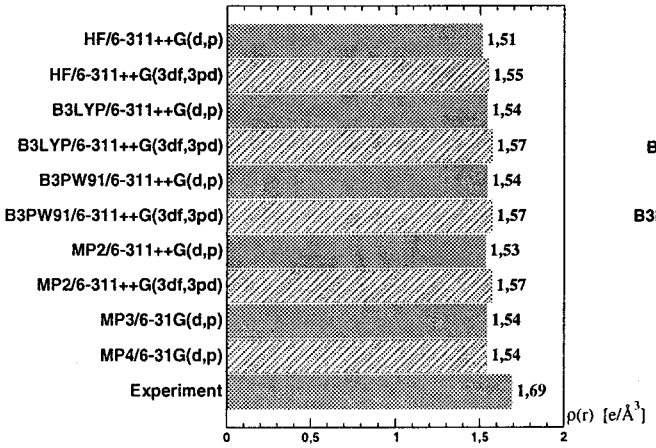

$\overline{x} = -8.8(32), e/a = 0.367$

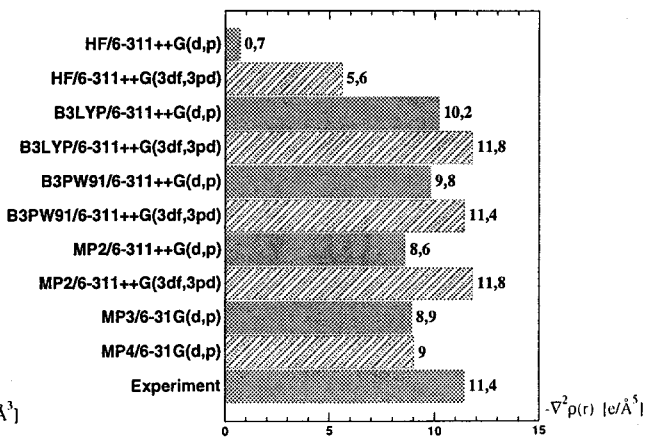

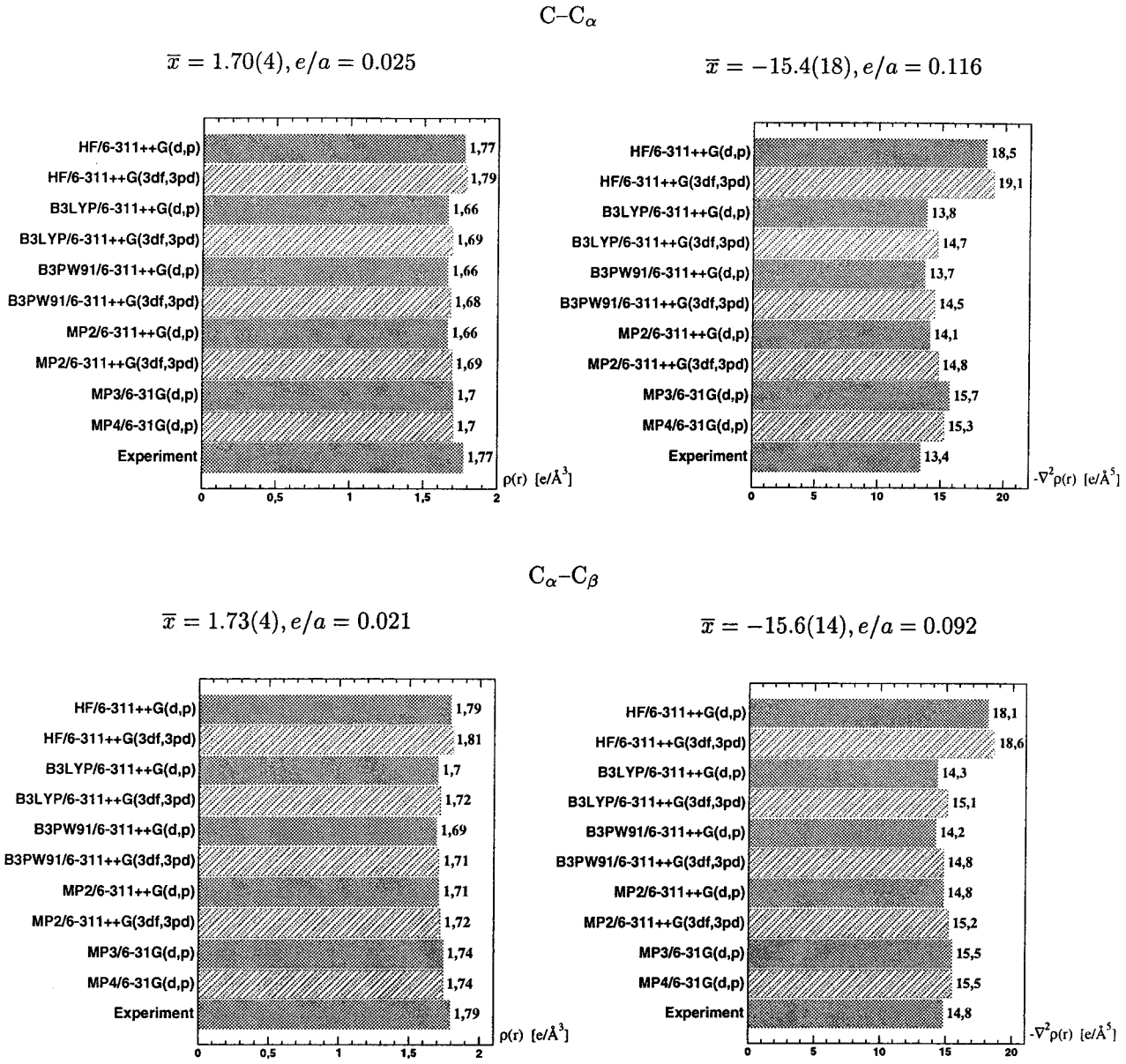

Figure 4. Comparison of bond topological parameters for serine. $\rho(\mathbf{r}_{BCP})$ and $-\nabla^2\rho(\mathbf{r}_{BCP})$ are plotted for 10 theoretical calculations using different levels of approximation and differrent basis sets. Experimental results are also shown. The theoretical calculations have been performed at the experimental geometry. The $\bar{x}$-values are the averages of the 10 theoretical values (including ESDs in parentheses). The *e*/*a* (ESD/average) ratios are a relative measure of the spread of the theoretical results.

the Gaussian98 program package[30] at the Hartree−Fock (HF) and DFT level of theories (with the popular B3LYP functional) and experimental geometry, utilizing the 6-311++G(3df,3pd) basis set. The topology of the theoretical densities were analyzed with the aid of the program package AIMPAC.[31,32]

Table 2 shows BTPs for bonds common to all amino acids, each averaged over 13 samples (except for the bond $C_\alpha-C_\beta$ which is absent in glycine) based on charge density studies of zwitterionic amino acids from the groups of Destro (L-Ala, Gly), Coppens (DL-His), by Arnold et al. (L-Asn·H_2O) and studies performed in our group on L-Asn·H_2O, DL-Asp, L-Gln, DL-Glu·H_2O, DL-Lys·HCl, DL-Pro·H_2O, DL-Ser, L-Thr, DL-Val. The data includes four amino acids/five data sets more than in our previous study[14] (Tables S1−S6, as suplementary material, contain all BTPs for the six amino acids L-Asn·H_2O, DL-Glu·H_2O, DL-Lys·HCl, DL-Pro·H_2O, DL-Ser, and DL-Val). The statistical errors are rather small for $\rho(\mathbf{r}_{BCP})$ and moderate for $\nabla^2\rho(\mathbf{r}_{BCP})$. For the former quantity the experimental variance/mean ratio lies between 3.0% (N−C_α) and 4.8% ($C_\alpha-C_\beta$), while for the latter the variation is noticably higher and ranges from 10.1% (O(2)−C) to 19.4% (N−C_α). In the carboxylate group one usually finds a longer and a shorter C−O bond (denoted

(30) Frisch, M. J.; Trucks, G. W.; Schlegel, H. B.; Scuseria, G. E.; Robb, M. A.; Cheeseman, J. R.; Zakrzewski, V. G.; Montgomery, J. A., Jr.; Stratmann, R. E.; Burant, J. C.; Dapprich, S.; Millam, J. M.; Daniels, A. D.; Kudin, K. N.; Strain, M. C.; Farkas, O.; Tomasi, J.; Barone, V.; Cossi, M.; Cammi, R.; Mennucci, B.; Pomelli, C.; Adamo, C.; Clifford, S.; Ochterski, J.; Petersson, G. A.; Ayala, P. Y.; Cui, Q.; Morokuma, K.; Malick, D. K.; Rabuck, A. D.; Raghavachari, K.; Foresman, J. B.; Cioslowski, J.; Ortiz, J. V.; Stefanov, B. B.; Liu, G.; Liashenko, A.; Piskorz, P.; Komaromi, I.; Gomperts, R.; Martin, R. L.; Fox, D. J.; Keith, T.; Al-Laham, M. A.; Peng, C. Y.; Nanayakkara, A.; Gonzalez, C.; Challacombe, M.; Gill, P. M. W.; Johnson, B. G.; Chen, W.; Wong, M. W.; Andres, J. L.; Head-Gordon, M.; Replogle, E. S.; Pople, J. A. *Gaussian 98*, revision A.7; Gaussian, Inc.: Pittsburgh, PA, 1998.
(31) Biegler-König, F.; Bader, R. F. W.; Tang, T.-H. *J. Comput. Chem.* **1982**, *3*, 317−328.
(32) Cheeseman, J.; Keith, T. A.; Bader, R. F. W. AIMPAC Program Package; McMaster University: Hamilton, Ontario, 1992.

Table 3. Nonbonded Valence Shell Charge Concentrations (VSCC)[a]

	atom (X)	$\rho(r_c)$		$\nabla^2\rho(r_c)$		*R*		At1–X–CP		CP_1–X–CP_2	
Asn	O(1)	6.01	6.33	−111.7	−149.3	0.348	0.341	109.2	140.4		
		6.18	6.52	−118.8	−154.8	0.345	0.339	106.8	112.8	142.5	102.5
	O(2)	6.09	6.29	−115.8	−146.5	0.347	0.342	108.8	104.2		
		6.18	6.31	−119.0	−143.2	0.345	0.341	106.3	92.8	144.9	162.0
Glu	O(1)	6.04	6.51	−113.1	−142.2	0.348	0.338	108.7	82.1		
		6.22	6.67	−120.6	−164.8	0.345	0.337	108.4	113.4	142.9	163.8
	O(2)	6.19	6.57	−120.2	−142.4	0.345	0.338	106.2	81.8		
		6.14	6.50	−118.1	−149.8	0.346	0.338	108.4	115.4	145.4	162.3
Lys	O(1)	6.20	6.09	−120.0	−131.9	0.345	0.344	107.9	146.7		
		6.03	5.84	−112.6	−122.9	0.348	0.348	109.1	110.2	143.0	99.9
	O(2)	6.17	6.33	−119.4	−152.0	0.345	0.342	108.6	100.2		
		6.23	6.46	−122.1	−145.3	0.344	0.341	106.1	85.7	145.4	172.5
Pro	O(1)	6.03	6.56	−112.8	−165.4	0.348	0.340	108.0	84.9		
		6.20	6.71	−120.2	−183.2	0.345	0.338	107.7	105.8	144.3	168.6
	O(2)	6.13	6.60	−117.4	−163.7	0.346	0.340	109.1	63.6		
		6.19	6.98	−119.8	−204.5	0.345	0.336	107.0	116.0	143.9	174.7
Ser	O(1)	6.03	6.20	−112.7	−133.5	0.348	0.341	108.6	105.0		
		6.21	6.25	−120.3	−137.7	0.345	0.341	108.0	111.0	143.5	143.6
	O(2)	6.13	5.94	−117.5	−114.6	0.346	0.344	108.9	102.3		
		6.19	5.95	−119.7	−121.3	0.345	0.344	106.4	113.6	144.8	143.2
Val	O(1)	6.21	6.28	−120.7	−134.6	0.345	0.341	106.4	109.6		
		6.16	5.81	−118.9	−110.4	0.346	0.347	108.6	103.8	145.0	92.7
	O(2)	6.19	6.15	−119.5	−139.0	0.346	0.344	108.1	124.8		
		6.03	5.90	−112.7	−110.7	0.351	0.346	108.9	127.1	143.6	97.3

[a] In each column entries on the left correspond to theory (HF/6-311++G(3df,3pd)), entries on the right to experimental results. *R* denotes the distance of the (3, +3) critical point of $\nabla^2\rho(\mathbf{r})$ to the corresponding atom X, At1−X−CP is the angle which is defined by the At1−X and X−CP vectors. CP_1−X−CP_2 is the angle defined by the CP_1−X and X−CP_2 vectors.

by O(1)−C and O(2)−C, respectively) which is due to the different crystal environment (hydrogen bonding) of the oxygen atoms. We find here that although the average BTPs correlate well with the bond distances the differences lie in the range of standard deviations. The average value of $\rho(\mathbf{r_{BCP}})$ of 2.71/2.83 e/Å^3 for these bonds is consistently higher than that for the C−O(H) bonds found in Ser and Thr but lower than that for the carbonyl type C═O bonds in Asn, Asp, Gln, and Glu.[12−14,17]

The theoretical $\rho(\mathbf{r_{BCP}})$ and $\nabla^2\rho(\mathbf{r_{BCP}})$ values scatter in a narrower range than the experimental ones with the exception of the (N−C_α) bond.[33] This statement, though in a limited sense, also applies to the basis-set dependence of the above properties. In this case, as it is demonstrated for Ser (Figure 4), the variance/mean values for the electron density are slightly lower for all bonds than the corresponding experimental ones. This holds also for the Laplacians of the C−C_α and C_α−C_β bonds but not for the polar O−C and N−C_α bonds. A good agreement between theory and experiment is found for the two negative curvatures λ_1 and λ_2. However, the discrepancies in the positive curvature (λ_3) in polar bonds often exceeds 50%. We note that for most of the bonds the principal curvatures calculated at the DFT level are closer to the experimental values than those predicted by the HF theory. The same conclusion can be drawn for the Laplacian. In contrast, it is the HF method that gives a closer result to the experimental one if $\rho(\mathbf{r_{BCP}})$ is considered. The inconsistency in the bond curvatures was recognized in earlier studies on aspartic acid,[12] proline,[2] and asparagine[14,17] and was partly attributed to the discrepancy between the theoretical and experimental locations of the BCP's. Indeed, the HF/6-311++G(3df,3pd) BTP's evaluated at the experimental BCP's resemble closely in value to those extracted from the X-ray data.[33] Volkov et al.[11] have recently discussed the inadequacy of the deformation radial functions to reproduce fine details of the density along the bond path. To see the extent to which their findings apply to the amino acids of this study we generated static structure factors for Ser from the B3LYP/6-311++G(3df,3pd) wave function (isolated molecule at the experimental geometry) and performed a multipole refinement on this simulated data similar to that used to treat the experimental data ($R = 0.06\%$). The topological analysis of the density obtained led to bond descriptors similar to the exact ones, except for the parallel curvatures. These indices for the carbonyl bonds, as derived from the fitted density, were found to be about half of those obtained directly. For all other bonds, the model overestimated λ_3 by up to 90%. A slightly better agreement was achieved if the κ' parameters were included in the refinement.

4.2. Nonbonded Valence Shell Charge Concentrations. Critical points of the Laplacian distribution bear chemical significance in the topological theory of molecular structure. Nonbonded VSCC's, identified as (3, +3) critical points of $\nabla^2\rho(\mathbf{r})$, can be interpreted as the free electron pairs of the valence shell electron pair repulsion (VSEPR) model[3]. The location and characterization of the VSCCs in X-ray charge densities is a very demanding numerical task since an accurate estimation of the fourth derivatives of the electron density is required. For the six amino acids discussed above we could locate and characterize all expected nonbonded VSCCs. Table 3 lists related parameters (derived from the model densities and from HF/6-311++G(3df,3pd) wave functions of the isolated molecules at the experimental geometry) for the oxygen atoms in the carboxylate groups. In L-Asn·H_2O, DL-Glu·H_2O, DL-Pro·H_2O, and DL-Ser there are additional VSCCs associated with the oxygen atoms in C═O and O−H groups (nonbonded VSCCs were also found at the amide nitrogen of L-Asn·H_2O, but they are not included in the table). The experimental and theoretical distances of each VSCC from the corresponding nucleus are practically identical which, however, does not imply perfect match in their location. In the isolated molecule the CP_1−O−

(33) Flaig, R. Ph.D. Thesis, Freie Universität Berlin, 2000.

Table 4. Hydrogen Bonds and Weak Interactions[a]

	A···H–D	symmetry	R(A···D)	R(A···H)	α(A···H- -D)	$\rho(\mathbf{r}_c)$	$\nabla^2\rho(\mathbf{r}_c)$
L-Asn···H_2O	O(1)···H(1)−N(1)	$1/2 + x, -1/2 - y, -z$	2.8044(4)	1.86(3)	157.1	0.24(4)	3.3(3)
	O(1)···H(6)−C(3)	$-1/2 - x, -y, -1/2 + z$	3.4620(3)	2.5573(2)	140.4	0.03(1)	0.7(1)
	O(1)···H(7)−N(2)	$-1/2 - x, -y, -1/2 + z$	3.2673(5)	2.5347(4)	130.4	0.05(1)	0.7(1)
	O(1)···H(7)−N(2)	$-x, -1/2 + y, 1/2 - z$	2.9821(3)	2.1869(3)	136.0	0.09(1)	1.6(1)
	O(2)···H(8)−N(2)	$1/2 - x, -y, -1/2 + z$	2.9089(5)	1.9155(3)	176.0	0.11(2)	3.4(2)
	O(2)···H(9)−O(4)	x, y, z	2.8105(5)	1.9364(3)	169.8	0.18(1)	2.6(1)
	O(2)···H(10)−O(4)	$-1/2 + x, 1/2 - y, -z$	2.7891(4)	1.9434(3)	159.7	0.18(2)	2.6(1)
	O(3)···H(2)−N(1)	$1+x, y, z$	2.7873(5)	1.7719(3)	165.4	0.19(4)	4.2(1)
	O(3)···H(5)−C(3)	$-x, -1/2 + y, 1/2 - z$	3.3369(3)	2.4131(3)	142.6	0.03(1)	0.7(1)
	O(4)···H(3)−N(1)	$-x, 1/2 + y, 1/2 - z$	2.8306(3)	1.9353(2)	143.2	0.14(1)	2.6(1)
	O(4)···H(4)−C(1)	$1 + x, y, z$	3.3068(4)	2.3891(3)	142.5	0.05(1)	1.0(1)
DL-Glu···H_2O	O(1)···H(2)−N(1)	$x, -1/2 - y, 1/2 + z$	2.7487(4)	1.7175(3)	170.7	0.23(1)	4.8(1)
	O(1)···H(4)−C(1)	$-1/2 + x, y, -1/2 - z$	3.3038(4)	2.5713(4)	124.4	0.05(1)	0.7(1)
	O(1)···H(5)−C(3)	$-1/2 + x, y, -1/2 - z$	3.2733(5)	2.5769(4)	121.0	0.04(1)	0.7(1)
	O(2)···H(3)−N(1)	$1/2 + x, y, -1/2 - z$	2.8020(4)	1.7988(4)	160.9	0.17(1)	3.7(1)
	O(2)···H(7)−C(4)	$1/2 + x, y, -1/2 - z$	3.4794(4)	2.4234(3)	162.9	0.03(1)	0.8(1)
	O(2)···H(9)−O(4)	$-1/2 - x, -1 - y, 1/2 + z$	2.5629(4)	1.6800(3)	171.3	0.42(2)	2.6(1)
	O(3)···H(10)−O(5)	$-1/2 - x, -1 - y, -1/2 + z$	2.8271(5)	1.9387(4)	175.4	0.15(1)	2.6(1)
	O(4)···H(4)−C(1)	$-1/2 - x, -1/2 + y, z$	3.4614(5)	2.6981(4)	127.4	0.03(1)	0.5(1)
	O(4)···H(11)−O(5)	x, y, z	2.9546(5)	2.0649(3)	177.6	0.12(1)	2.0(1)
	O(5)···H(1)−N(1)	$-1 - x, -1/2 + y, -1/2 - z$	2.8192(5)	1.8135(4)	161.6	0.17(1)	3.6(1)
DL-Lys···HCl	O(1)···H(3)−N(1)	$-1 - x, 1 - y, 1 - z$	2.8512(7)	1.8203(5)	170.4	0.15(2)	4.0(2)
	O(2)···H(1)−N(1)	$x, 3/2 - y, 1/2 + z$	2.8128(7)	1.7980(5)	164.2	0.16(1)	4.1(2)
	O(2)···H(14)−N(2)	$-1 - x, 1 - y, 2 - z$	2.8658(6)	1.8617(5)	161.3	0.14(1)	3.6(2)
	Cl(1)···H(2)−N(1)	$-x, 1 - y, 1 - z$	3.3818(5)	2.5856(1)	133.1	0.07(1)	1.0(1)
	Cl(1)···H(15)−N(2)	$-x, 1/2 + y, 3/2 - z$	3.1770(5)	2.1710(1)	162.1	0.14(1)	2.5(1)
	Cl(1)···H(13)−N(2)	$-x, 1 - y, 2 - z$	3.1705(4)	2.1410(1)	170.1	0.14(1)	2.8(1)
DL-Pro···H_2O	O(1)···H(2)−N(1)	$1 + x, y, z$	2.7346(5)	1.9102(7)	164.7	0.28(2)	3.2(1)
	O(1)···H(1)−N(1)	$-x, 1 - y, -z$	2.8520(6)	2.2225(8)	130.7	0.13(1)	1.7(1)
	O(1)···H(3)−C(2)	$1/2 + x, 3/2 - y, -z$	3.4554(7)	2.5981(4)	143.8	0.06(1)	0.8(1)
	O(2)···H(10)−O(3)	$1/2 - x, 1/2 + y, z$	2.8422(7)	1.9408(6)	175.7	0.14(2)	2.8(1)
	O(2)···H(3)−C(2)	$1 + x, y, z$	3.3025(6)	2.6611(6)	122.1	0.06(1)	0.8(1)
	O(3)···H(11)−O(3)	$-1/2 + x, y, 1/2 - z$	3.0730(4)	2.1880(5)	170.6	0.06(1)	1.5(1)
	O(3)···H(9)−C(3)	$-x, -1/2 + y, 1/2 - z$	3.4612(6)	2.5857(7)	143.2	0.04(1)	0.7(1)
	O(3)···H(6)−C(4)	$1/2 + x, y, 1/2 - z$	3.4258(7)	2.4413(6)	153.2	0.05(1)	0.9(1)
DL-Ser	O(1)···H(4)−O(3)	$1/2 - x, -1/2 + y, 1 - z$	2.6630(3)	1.6544(2)	174.6	0.25(1)	5.5(2)
	O(1)···H(2)−C(2)	$x, y, 1 + z$	3.2822(2)	2.2087(2)	173.0	0.06(1)	1.5(1)
	O(2)···H(12)−N(1)	$1/2 - x, -1/2 + y, -z$	2.7984(3)	1.8039(2)	158.7	0.18(2)	3.6(2)
	O(2)···H(13)−N(1)	$1/2 - x, -1/2 + y, 1-z$	2.8550(3)	1.8224(2)	170.9	0.17(2)	3.6(1)
	O(3)···H(11)−N(1)	$-1/2 + x, 1/2 - y, z$	2.7649(3)	1.7711(2)	158.3	0.21(1)	4.1(1)
DL-Val	O(1)···H(3)−N(1)	x, y, z	2.8785(2)	1.8541(1)	167.6	0.15(2)	3.6(1)
	O(1)···H(1)−N(1)	$-x, 2 - y, -z$	2.9487(3)	1.9553(2)	158.7	0.12(1)	2.8(1)
	O(2)···H(2)−N(1)	$x, -1 + y, z$	2.7526(2)	1.7132(1)	177.4	0.25(2)	5.0(2)

[a] R(A···D), R(A···H), and R(A−CP) denote the distances to the acceptor atom, donor atom, H ·atom, and critical point, respectively of the A···H interaction. α(A···H−D) is the angle which is defined by the acceptor, hydrogen, and donor atom. Units: ρ(e/Å^3), $\nabla^2\rho$(e/Å^5).

CP_2 angle (143−145°) is larger than the C−O−CP angle (106−109°), in accord with the VSEPR model[34,35] which postulates a higher steric demand for lone-pair electrons than bonded electron pairs. For the crystalline density the corresponding angles are in the range of 92.7−174.7° and 63.6−146.7°, respectively. These observations reflect the strong impact of intermolecular interactions in the crystalline environment. The electron density differences at these sites lie, with one exception (Pro 11%), below 7%, while for the Laplacian the discrepancies spread in a wide range between 3 and 41%. A remarkably good agreement is found for Ser and Val where the maximum difference for $\nabla^2\rho(\mathbf{r})$ is 16% and 14% respectively. This might be due to the very high resolution of the two data sets ($\sin\theta/\lambda > 1.5$ Å^{-1}).

4.3. Topology of the Hydrogen Bonds. There has been extensive previous work on hydrogen bonding on the basis of distances and angles, hence on geometrical criteria. A considerable part of these efforts, especially concerning weak interactions, is summerized in ref 36, where, for example, a classification and detailed characterization of C−H···O interactions is given. Topological analyses of charge density distributions provide additional topological parameters of intermolecular interactions and can therefore lead to a deeper insight into the strength of these interactions.

Geometrical and topological hydrogen-bond parameters for the amino acids L-Asn·H_2O, DL-Glu·H_2O DL-Lys·HCl, DL-Pro·H_2O, DL-Ser, and DL-Val are listed in Table 4 (see also Tables S7−S12). Only those interactions are included for which the acceptor−hydrogen distance (A···H−X, where X = O, N, C, and A = O, Cl) is less than the sum of their van der Waals radii. A total number of 43 such interactions was found (8 O···H−O, 20 O···H−N, 12 O···H−C, and 3 Cl···H−N). A relatively low value of the electron density and a positive value for the Laplacian at the BCP, observed in all cases, are

(34) Gillespie, R. J. *Molecular Geometry*; Van Nostrand Reinhold: London, 1972.
(35) Bader, R. F. W.; Gillespie, R. J.; MacDougall, P. J. *J. Am. Chem. Soc.* **1988**, *110*, 7329−7336.
(36) Desiraju, G. R.; Steiner, T. *The Weak Hydrogen Bond*; Oxford University Press: New York, 1999.

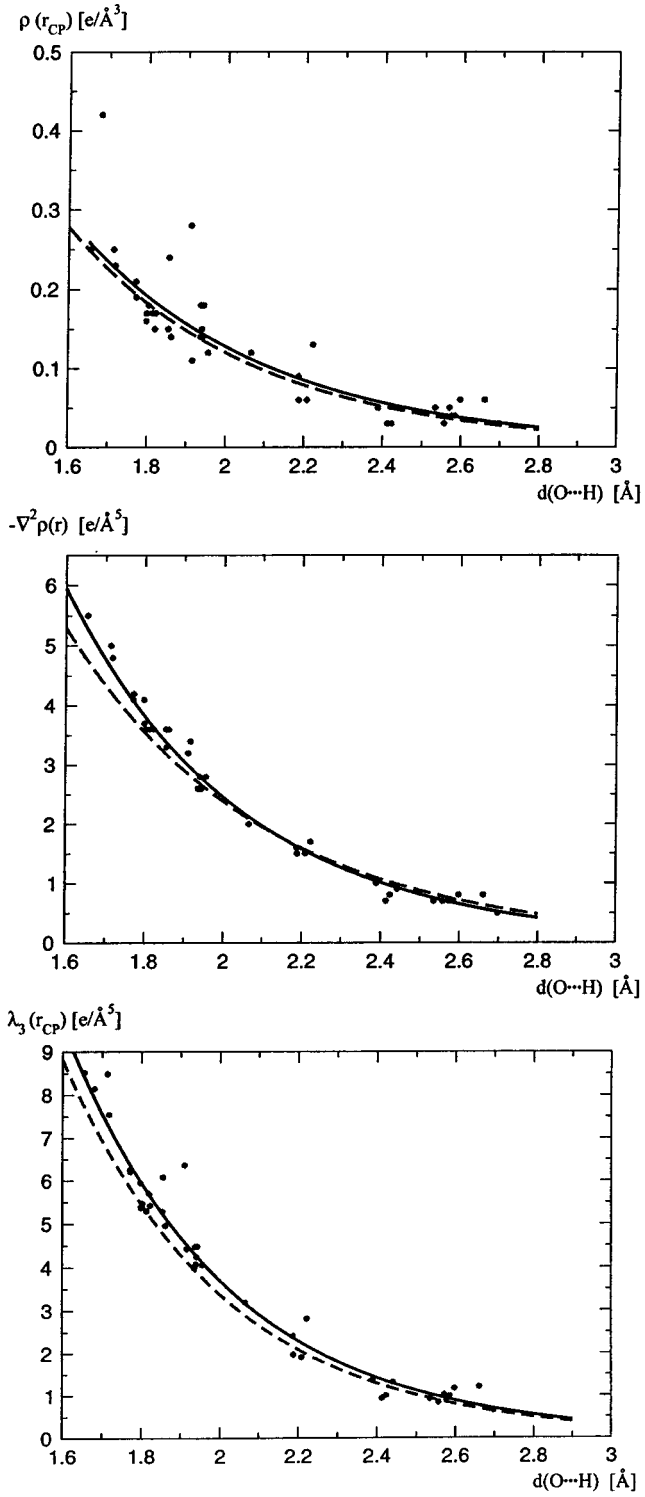

Figure 5. Plots of the electron density ($\rho(\mathbf{r_{BCP}})$), Laplacian ($\nabla^2\rho(\mathbf{r_{BCP}})$), and the positive curvature λ_3 against the distance d(O···H) of the O···H interaction for the hydrogen bonds found in the six amino acids L-Asn·H_2O, DL-Glu·H_2O, DL-Lys·HCl, DL-Pro·H_2O, DL-Ser and DL-Val. The solid curve is a fit by an exponential function, the dashed curve is from ref 37.

characteristic for closed-shell interactions. The geometrical and topological indices show clear trends when going from the relatively strong O···H−O through the O···H−N hydrogen bond of medium strength to the weak O···H−C interaction.[36] The acceptor−hydrogen distance R(A···H) is in the range of 1.6544−2.0649, 1.7132−2.5347, and 2.2087−2.6981 Å for the hydrogen bonds in the above order. The angle α(A···H−D) for the O···H−O interaction is found between 159.7 and 177.6°. This range is much broader for the weaker interactions (O···H−N: 130.4−177.4°, O···H−C: 121.0−173.0°. The $\rho(\mathbf{r_{BCP}})$ values exceed 0.1 e/Å^3 for the O···H−O (0.06−0.42 e/Å^3) and O···H−N (0.05−0.28 e/Å^3) interactions, while they lie below that for the O···H−C (0.03−0.06 e/Å^3) contacts studied here. The Laplacian in turn is significantly lower in value for the weak O···H−C (0.5−1.5 e/Å^5) than for the stronger O···H−O (1.5−5.5 e/Å^5) and O···H−N (0.7−5.0 e/Å^5) hydrogen bonds. This behavior is also reflected in the positive curvature λ_3. For example, the minimum value for the O···H−O hydrogen bond (1.97−8.52 e/Å^5) is higher than the maximum value for the O···H−C interaction (0.65−1.91 e/Å^5). In the former case the critical point is found to lie almost on the O−H vector which is indicated by the distance of R(CP-bond) (see Tables S7−S12) being in the range of 0.010−0.063 Å. In the other two cases the CP displacements are found to be in a much higher range, amounting up to about 0.4 Å.

On the basis of experimental data for 83 hydrogen bonds occurring in 15 different compounds Espinosa et al. established fundamental correlations between geometrical, topological and energetic parameters.[37,38] The data analyzed were drawn from experiments on different organic compounds performed in different laboratories under different experimental and refinement conditions. To explore the reproducibility of their results we repeated their analysis but using the data of 40 intermolecular O···H−X (X = O, N, C) type hydrogen bonds present in the crystal structures of the six amino acids considered in this study. Figure 5 shows the plots of the electron density, the Laplacian and the positive curvature λ_3 versus the O···H distance. In all cases an exponential correlation is observed. The solid line corresponds to a fit by a simple exponential function the parameters of which are in a very good agreement with those given in reference 37. The agreement in terms of the positive curvature λ_3 is especially good. The results support the description of hydrogen bonds being of mainly electrostatic nature.[37,38] Indeed, all outliers of the fit can be identified as hydrogen bonds with a considerable covalent character.

5. Conclusions

In this report we demonstrate the feasibility of comparative experimental charge density studies on an entire class of chemically related compounds. Topological properties of densities extracted from high resolution and precision X-ray data for six amino acids (L-Asn·H_2O, DL-Glu·H_2O, DL-Lys·HCl, DL-Pro·H_2O, DL-Ser, and DL-Val) were determined and compared with those obtained earlier for other amino acids and those derived from ab initio wave functions. Despite varying experimental and refinement conditions, different β-substituents and crystal environments, the results are fairly consistent. The theory versus experimental comparison reveals that among the BTPs examined $\rho(\mathbf{r_{BCP}})$ and the perpendicular curvatures can reliably be obtained from X-ray data. The experimental ESDs calculated with reference to the mean of the amino acid sample is considerably higher than those derived directly from the errors of the least-squares variables for each compound. The former quantity seems

(37) Espinosa, E.; Souhassou, M.; Lachekar, H.; Lecomte, C. *Acta Crystallogr., Sect. B* **1999**, *B55*, 563−572.
(38) Espinosa, E.; Lecomte, C.; Molins, E. *Chem. Phys. Lett.* **1999**, *300*, 745−748.

to provide an estimation for the uncertainty and transferability of the experimental properties that is more realistic than the latter one.

The inconsistency in the bond-parallel curvatures for the polar bonds has been observed earlier and could be attributed to model inadequacies. Our results based on the density extracted from the simulated data of Ser also indicate that the deformation radial functions (single-ζ functions with energy-optimized exponents) are not flexible enough to account for fine details of the bond density. We should mention, however, that the variance in experimental $\rho(\mathbf{r_{BCP}})$ and $\nabla^2\rho(\mathbf{r_{BCP}})$ values for the C−C bonds is in the range of the variance found for these properties by different theoretical methods utilizing different basis sets. For the Laplacian of the polar O−C and N−C_α bonds the spread derived from the multipole model is considerably narrower than the one obtained from theory. The experimental Laplacian at the nonbonded VSCCs scatter around the theoretical ones but in a very wide range. This observation raises the question of how reliably VSCC properties can be derived from X-ray data. Periodic ab initio calculations on urea have shown that a drastic rearrangement of the valence shell of the keto oxygen atom took place upon hydrogen bond formation in the crystal.[39] The effect of intermolecular interactions (hydrogen bonds) on the density appears to be enhanced if viewed in terms of the Laplacian. In some cases it was found that the C−O−CP angle is correlated with the geometry of the hydrogen bond.

Acknowledgment. Funds were gratefully accepted from the Bundesminister für Forschung und Technologie (BMBF, Grant 05 SM8KEA0), the Deutsche Forschungsgemeinschaft, grant Lu 222/22-1 and the Fonds der Chemischen Industrie.

Supporting Information Available: Tables of additional data (PDF). This material is available free of charge via the Internet at http://pubs.acs.org.

JA011492Y

(39) Gatti, C.; Saunders: V. R.; Roetti, C. *J. Chem. Phys.* **1994**, *101*, 10686−10696.